ZnO Microrod Arrays Grown on Copper Substrates as Anode Materials for Lithium Ion Batteries

X. H. Huang[*]*, J. B. Wu*[*]*, Y. Lin, R. Q. Guo*

College of Physics & Electronic Engineering, Taizhou University, Taizhou 318000, China
[*]E-mail: drhuangxh@hotmail.com; wujb@tzc.edu.cn

ZnO microrod arrays are prepared on copper substrate by a simple chemical bath deposition method. The arrays are characterized by means of X-ray diffraction (XRD), scanning electron microscopy (SEM), and transmission electron microscopy (TEM). As anode materials of lithium ion batteries, their electrochemical performances are investigated by cyclic voltammetry (CV) and galvanostatic charge-discharge cycle tests. The electrochemical test results show that ZnO microrod arrays not only have an initial coulombic efficiency of 78.5% and a reversible capacity above 600 mAh g^{-1}, but also exhibit enhanced cycling performance and rate capability. It is believed that the microrod array structure plays an important role in the electrochemical performance.

1. INTRODUCTION

3d transition-metal oxides (MO, M = Fe, Co, Ni, Cu, and Zn) are promising anode materials of lithium ion batteries whose reversible capacities are about 2~3 times higher than the traditional carbon-based materials [1–7]. Among these oxides, ZnO has a theoretical capacity of 978 mAh g^{-1}, and it also has some advantages such as low cost, easy preparation, and chemically stable, which should have been more attractive. However, up to now, ZnO materials is rarely studied as anode materials of lithium ion batteries, mainly attributed to its low practical capacity even less than carbon and very serious capacity fading during cycling. This is because ZnO is a low conductive material, and it suffers large volume change during the discharge–charge process which results in the loss of contact with the current collector. Some methods have been developed to improve the ZnO's electrochemical properties, for example, coating with metal or carbon layer [8–10], incorporating with compounds [11–

14], doping with Se [15], preparing nanostructured materials [16] and so on. But still up to now, no significant improvements have been achieved.

Binder-free electrodes are often prepared to obtain better electrochemical performances [17, 18]. These electrodes are usually composed of nanoflakes, nanorods, or nanotubes arrays, which are grown orderly on the current collector substrates. As having advantages of better electrical contact, larger electrochemical reaction interfaces, shorter diffusion lengths of lithium ions, and good accommodations for volume changes, these electrodes often exhibit better electrochemical performances than the common powder electrodes prepared by slurry coating process. However, because most of these binder-free electrodes are nanostructured, which contain low mass of active materials, they can only be used in micro lithium ion batteries, and increasing the mass of active materials by simply increasing the film thickness, density, or particles sizes often deteriorates the electrochemical performances.

In the present work, ZnO microrod arrays are grown on copper foil substrate by a simple chemical bath deposition technique without any templates or pre-growth of seed layers. Different from the nanostructured electrodes, this binder-free electrode is constructed by microsized ZnO rod arrays and can contain much more active materials. As anode materials of lithium-ion batteries, their electrochemical properties are studied in detail.

2. EXPERIMENTAL

ZnO microrod arrays were deposited on a copper foil by a simple chemical bath deposition technique. The deposition solution was mixed by 0.04 mol zinc acetate dihydrate, 0.5 mL ethylenediamine, and 150 mL distilled water. A copper foil, ultrasonic cleaned with acetone and ethanol, was used as the substrate and suspended horizontally in the solution. The solution was mildly stirred and its temperature was maintained at 65 ^{o}C. The deposition process was lasted for 1 h, and subsequently, the copper foil was taken out, washed with distilled water and ethanol for several times. After dried, the foil was finally heated in a quartz tube furnace in flowing argon at 350 ^{o}C for 30 min.

The microstructure and morphology of the as-prepared sample was characterized by means of X-ray diffraction (XRD, Bruker D8 advance with Cu Kα radiation), scanning electron microscopy (SEM, Hitachi S-4800) and transmission electron microscopy (TEM, FEI Tecnai G2 F30).

To make a comparison, two kinds of working electrodes were prepared. The binder-free electrode directly used the copper foil supported ZnO microrod arrays as the working electrode, while the common powder electrode was prepared by a regular slurry coating procedure. The exact process was that, scraping the ZnO microrods from the copper foil substrate, mixing it with acetylene black and the N-methyl pyrrolidinone (NMP) solution of polyvinylidene fluoride (PVDF) to prepare slurry, and then spreading the slurry on the copper foil substrate. In the powder electrode, the mass ratio of ZnO, acetylene black and PVDF is 80:12:8.

CR2025-type coin cells were assembled in a dry argon-filled glove box (Mikrouna Super). Both of the water and oxygen concentrations in the glove box were controlled below 1 ppm. Pure lithium wafer were used as the courter electrode. The two electrodes were separated by a Celgard 2300

membrane. The electrolyte was 1M LiPF$_6$ in ethylene carbonate (EC) and dimethyl carbonate (DMC) (1:1 by weight). The cells were sealed tightly in the glove box. Before measurements, all cells were aged for 12 h to ensure the electrodes and the membrane fully wetted by the electrolyte.

The discharge-charge cycling performances of the cells were tested on a program-controlled battery test instrument (LAND CT2001A). The cells are cycled at different current densities of 0.1, 0.5, 1 and 2 A g^{-1} between the two cut-off voltages of 0.02 and 3 V. Cyclic voltammetry (CV) tests were performed on an electrochemical workstation (CHI600D) using a sweep speed of 0.1 mV s^{-1} in the potential range of 0 ~ 3 V. All of the electrochemical tests were performed in a thermostatic room in which the temperature was kept at 25 °C.

3. RESULTS AND DISCUSSION
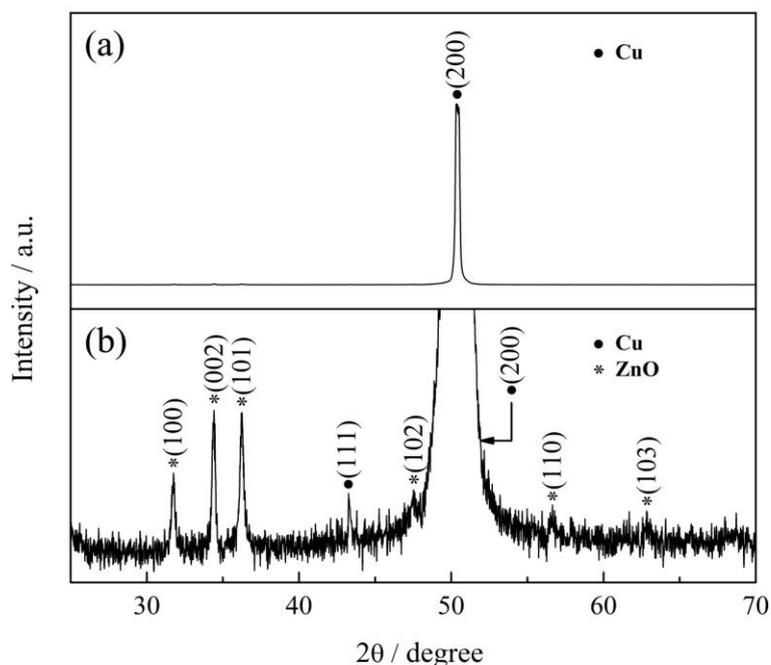
Figure 1. XRD pattern of ZnO microrod array deposited on copper foil, (a) the overall pattern, and (b) the magnified pattern.

Figure 1 is the XRD pattern of the product grown on the copper foil substrate. The overall pattern is presented in Figure 1a. It shows a very sharp peak at 50.5°, which can be assigned to the (200) plane of copper, according to the JCPDS, No. 04−0836. This indicates that the copper foil substrate has a preferred orientation. In the magnified pattern, as shown in Figure 1b, it can be seen several diffraction peaks. The peaks at 31.8°, 34.4°, 36.3°, 47.5°, 56.6° and 62.9° corresponds to the (100), (002), (101), (102), (110) and (103) planes of wurtzite-type hexagonal ZnO, according to the JCPDS, No. 36−1451. The other peak at 43.3° is related with the (111) plane of copper.

The typical SEM images of the copper foil supported ZnO is present in Figure 2. It is clear that the surface of the substrate is fully covered by ZnO microrod arrays (Figure 2a).

element	wt %	at %
O (K)	17.65	46.64
Zn (K)	76.11	49.21
Cu (K)	6.22	4.14
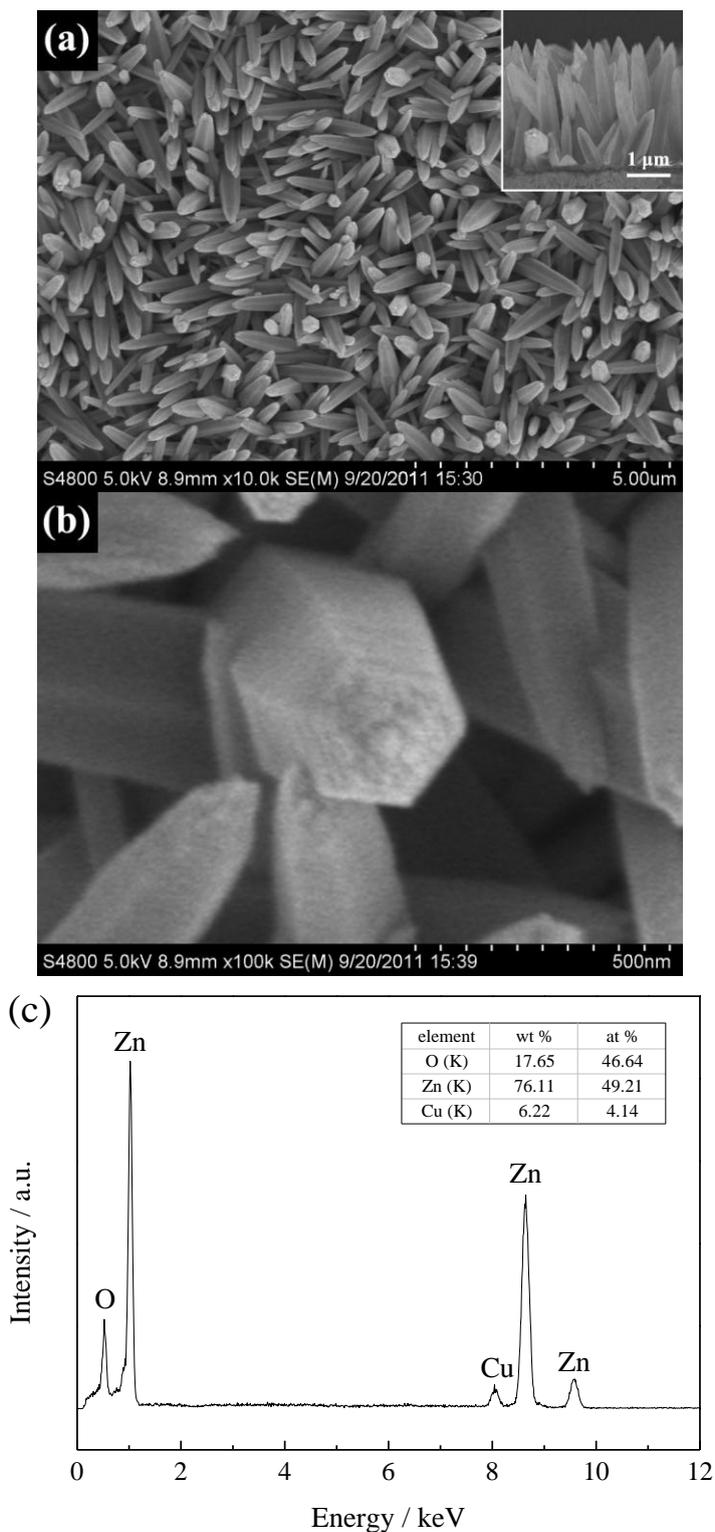
Figure 2. SEM results of the ZnO microrod array, (a) top-view image and the cross-sectional image, (b) the magnified image of a ZnO microrod, and (c) the EDS pattern of the ZnO microrod.

The insert cross-sectional image in the top right corner shows that ZnO microrods have a length of about 3 μm. These microrods grow directly on the substrate and most of them are nearly perpendicular to the substrate. This structure enables each microrod contact well with the copper foil substrate and has advantages of facilitating the charge transfer during the electrochemical reactions. According to the magnified SEM image, as shown in Figure 2b, the microrod is hexagonal columnar and has sharp tips. The EDS pattern (Figure 2c) exhibits Zn and O peaks and no other impurity peaks can be observed except the Cu peak originated from the copper foil substrate.
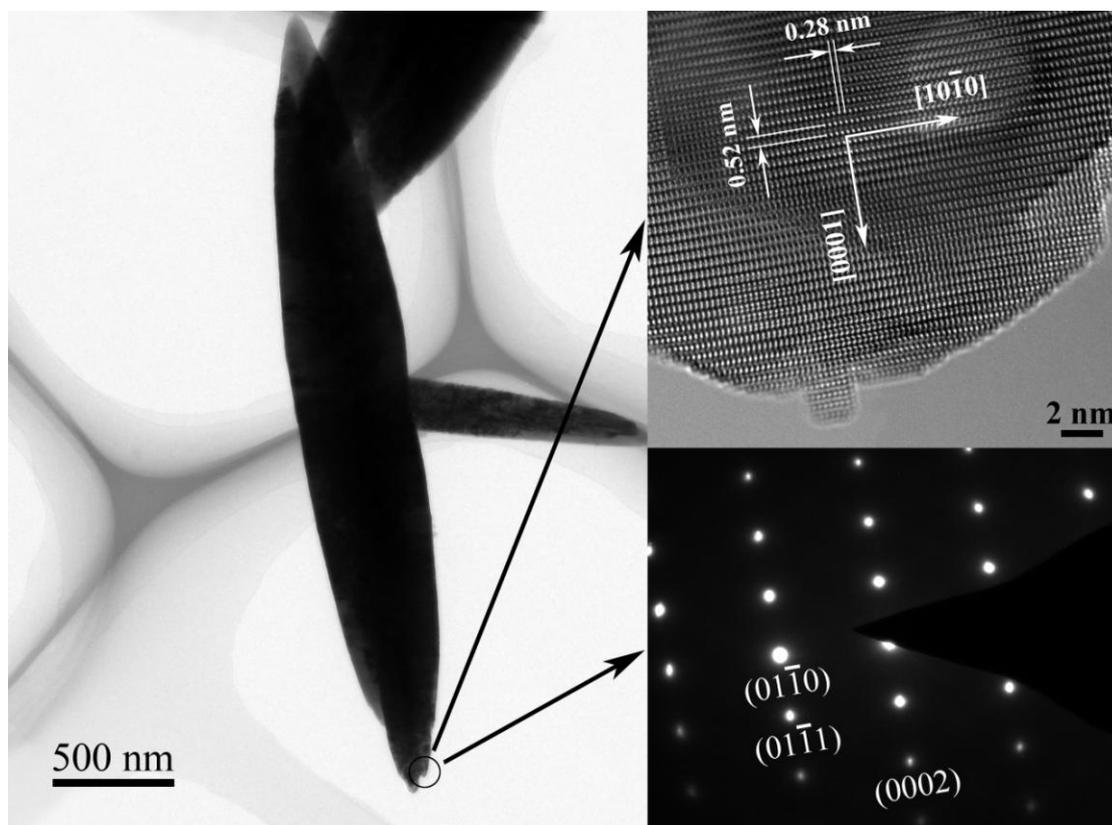
Figure 3. TEM results of a ZnO microrod, including an overall image of a single microrod, a high resolution image and the corresponding SAED pattern.

The microstructure of the ZnO microrod is further investigated by TEM (Figure 3). From the TEM image it is known that the microrod is about 3 μm in length and has sharp tips in both sides, which is in agreement with the SEM result. The top-right is the high-resolution image of the tip, and it reveals clear lattice spacings of 0.52 and 0.28 nm, corresponding to the interplanar spacings of the (0001) and $\{10\bar{1}0\}$ planes of ZnO, respectively. This also indicates that the ZnO microrod grows preferentially along the [0001] direction. The image in the low-right corner is the corresponding SAED pattern, indicating that the ZnO microrod is single-crystalline.

The electrochemical process of ZnO towards Li is more complicated than other transition-metal oxides, according to the previous studies [9, 11]. The first discharge process involves the decomposition of ZnO and the formation of Li-Zn alloy, which can be written as follows.

$$ZnO + 2Li \rightarrow Zn + Li_2O \qquad (1)$$

$$Zn + Li \rightarrow LiZn \qquad (2)$$
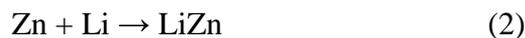
Subsequently, the following charge and discharge reaction are reversible, including two reactions as below.

$$LiZn \rightleftharpoons Zn + Li \qquad (3)$$

$$Zn + Li_2O \rightleftharpoons ZnO + 2Li \qquad (4)$$

As anode materials of lithium ion batteries, the electrochemical performance of copper foil supported ZnO microrod arrays were investigated. The electrode reactions were analyzed by CV tests using a sweep speed of 0.1 mV s^{-1} between 0 and 3 V.
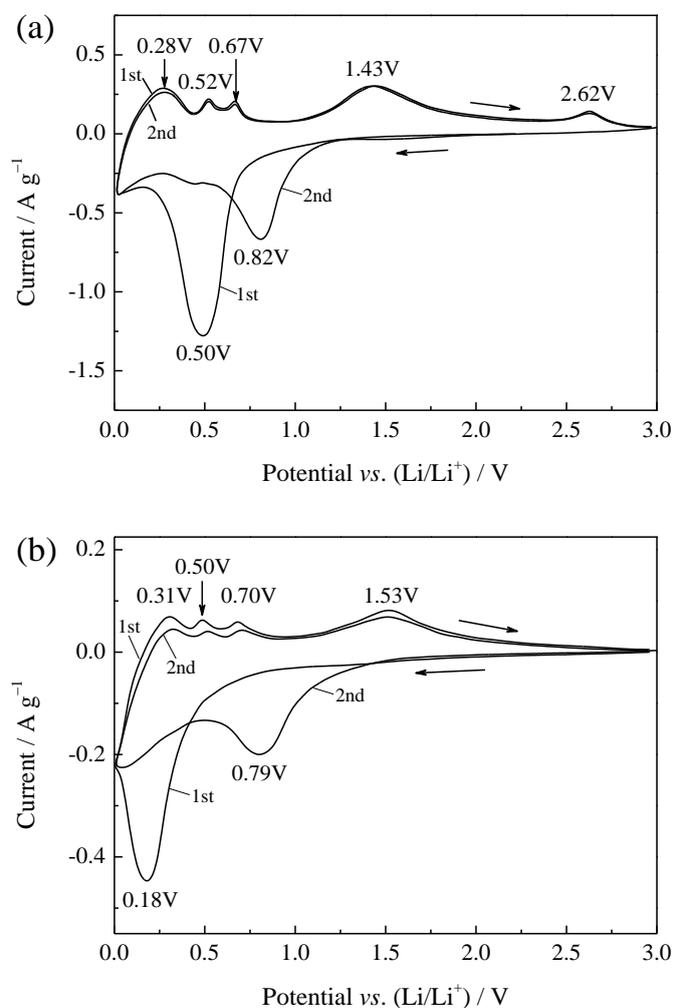
Figure 4. CV curves of (a) ZnO microrod array electrode and (b) ZnO microrod powder electrode at the sweep speed of 0.1 mV s^{-1}.

Figure 4 compares the CV curves of the ZnO microrod array electrode and the common ZnO powder electrode. For the array electrode (Figure 4a), there is a strong peak at about 0.5 V in the first cathodic curve. This peak is related to the first electrochemical process of ZnO, including the reduction of ZnO to Zn, the alloying reaction between Li and Zn, and the formation of the solid electrolyte interface (SEI) layer. The SEI layer is an organic-like layer consisting of ethylene-oxide-based oligomers, LiF, Li_2CO_3, and lithium alkyl carbonate ($ROCO_2Li$) [19]. The potentials of these electrochemical reactions are very close, so it shows only a strong reduction peak. In the subsequent anodic scan, the curve exhibits five peaks. The first four peaks, located at 0.28, 0.52, 0.67, and 1.43 V can be ascribed to the multi-step dealloying process of Li–Zn alloy. The last peak at 2.62 V corresponds to the oxidation process of Zn to ZnO [11]. In the second cycle, the reaction becomes more reversible. The cathodic peak shift to a higher potential of 0.82 V with decreased intensity and the anodic peaks coincide with those in the first scan. For the powder electrode (Figure 4b), the shape of curves are similar, but there are some differences in peak positions. Notice that no anodic peaks can be seen around 2.62 V, which indicates that in the powder ZnO electrode, the re-oxidation process of Zn back to ZnO, i.e. $Zn + Li_2O \rightarrow ZnO + 2Li$, may not occur at all. The reason should be that the ZnO microrods in the powder electrode cannot contact well with the substrate.
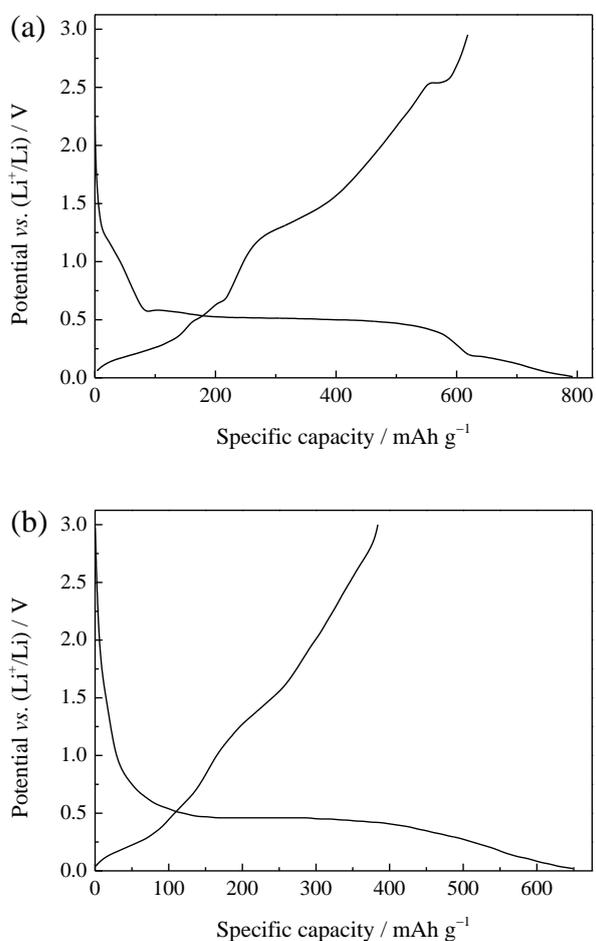
Figure 5. The first galvanostatic discharge-charge curve of (a) ZnO microrod array electrode and (b) ZnO microrod powder electrode at the same current density of 0.5 A g^{-1}.

Figure 5 compares the first galvanostatic discharge-charge curve of the two electrodes at the same current density of 0.5 A g^{-1}. The ZnO microrod array electrode (Figure 5a) delivers a first discharge capacity of 790 mAh g^{-1} and first charge capacity of 620 mAh g^{-1}. The initial coulombic efficiency is 78.5%, much higher than the reported value [8–16]. In contrast, the electrode made from ZnO microrod powders (Figure 5b) delivers much lower discharge and charge capacities, that is, 650 mAh g^{-1} and 385 mAh g^{-1}, exhibiting an initial coulombic efficiency of only 58.5%.

The enhanced capacities and initial coulombic efficiency of ZnO microrod array electrode can be ascribed to its more complete electrochemical reactions at the same current density. This can be concluded from their galvanostatic discharge-charge curves. It can be seen that the ZnO microrod array electrode exhibits much obvious plateaus than the ZnO microrod powder electrode. Especially worthy of notice, the plateau at about 2.6 V offers a charge capacity of about 40 mAh g^{-1}, while for ZnO microrod powder electrode, no plateaus can be seen around this potential at all, as with those in literature reports [8–16]. This plateau is in agreement with the CV curves, as both of the charge/discharge plateaus and the CV peaks are reflections of the electrochemical reactions.
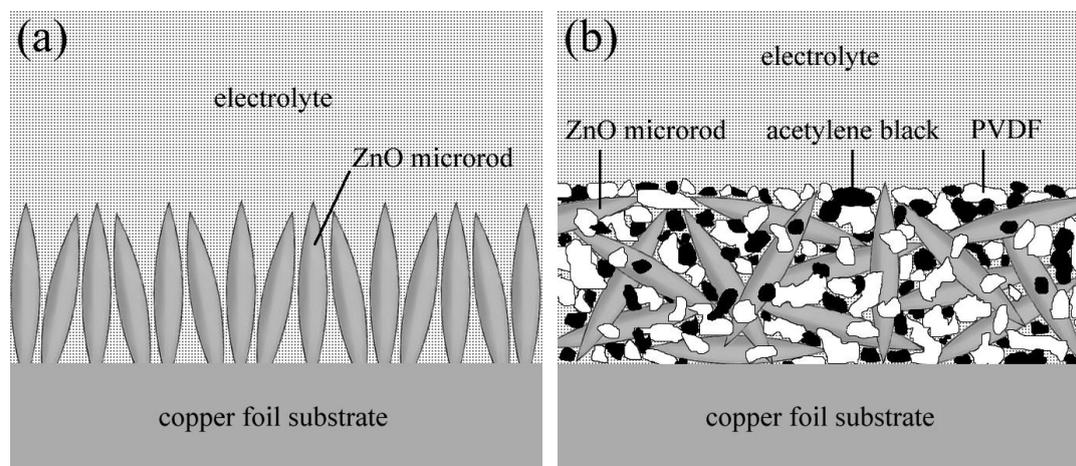
Figure 6. The structure diagrams of (a) ZnO microrod array electrode and (b) ZnO microrod powder electrode.

The more complete electrochemical reactions of ZnO microrod array electrode can be attributed to its microrod array structure. The structure diagrams of the two electrodes are presented in Figure 6. The array structure (Figure 6a) offers a larger specific surface area and enables each microrod contact well with the electrolyte. The increase of reaction interface reduces the current density per unit area and thus promotes the electrochemical reaction more fully. The array structure also enables each microrod contact well with the copper foil current collector, which facilitates the charge transfer and reduces the electrode polarization. For ZnO microrod powder electrode (Figure 6b), just as other common powder electrodes, these advantages do not exist. Therefore, the ZnO microrod array electrode exhibits enhanced capacities and initial coulombic efficiency.

Because of the improved electrical contact, the ZnO microrod array electrode also exhibits enhanced cycling performance. The discharge and charge capacities of the two electrodes at the same

current of 0.5 A g^{-1} are plotted in Figure 7. The ZnO microrod array electrode shows a stable capacity over 500 mAh g^{-1} after 100 cycles, over 80% of the initial value. In contrast, the ZnO microrod powder electrode shows a very rapid capacity fade, only about 150 mAh g^{-1} remains after 50 cycles.
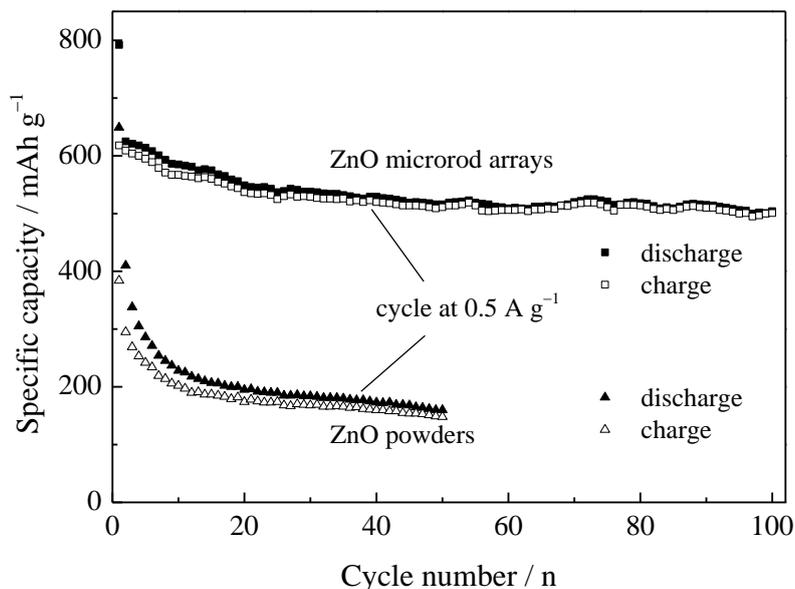
Figure 7. Cycling performance of the two electrodes at the same current density of 0.5 A g^{-1}.
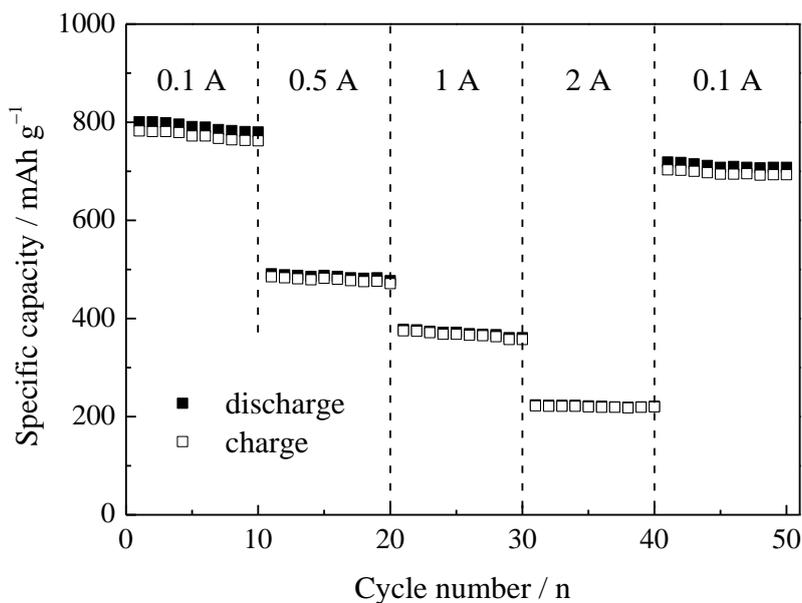
Figure 8. Rate capability of the ZnO microrod array electrode.

Finally, the rate capability of ZnO microrod array electrode was investigated, just using the same cell which had already been cycled 100 cycles. The cell was cycled at the current densities of 0.1, 0.5, 1, 2, and 0.1 A g^{-1} in turn, at each of which for 10 cycles, and the discharge and charge capacities

are plotted in Figure 8. When the electrode is cycled at the low current density of 0.1 A g^{-1}, it exhibits discharge and charge capacities of over 750 mAh g^{-1}. Lower capacities were obtained at the higher current density. Exactly, at the current densities of 0.5, 1, and 2 A g^{-1}, the capacities of each period are about 480, 370, and 220 mAh g^{-1}, respectively. At last, the current density returns back to the initial 0.1 A g^{-1}, the capacities can recover to the value of about 700 mAh g^{-1}. This means that the ZnO microrod array electrode has a relatively good rate capability, and this is originated from the enhanced electrical contact of the microrod array structure.

4. CONCLUSIONS

ZnO microrod arrays have been grown on the copper foil substrate by chemical bath deposition successfully. The hexagonal ZnO microrod is about 3 μm in length, and grows preferentially along [0001] direction. As anode materials of lithium ion batteries, this ZnO microrod arrays delivers initial coulumbic efficiency as high as 78.5% and a reversible capacity over 600 mAh g^{-1}. The arrays also exhibit good cycling performance and rate capability. The enhanced electrochemical performances are attributed to the microrod array structure, as this structure not only offers a larger specific surface area but also enables each microrod contact well with the electrolyte and the copper foil current collector.

References

1. P. Poizot, S. Laruelle, S. Dupont and J-M. Tarascon, *Nature*, 407 (2000) 496.
2. S. Grugeon, S. Laruelle, R. Herrera-Urbina, L. Dupont, P. Poizot and J-M. Trarscon, *J. Electrochem. Soc.*, 148 (2001) A285.
3. P. Poizot, S. Laruelle, S. Grugeon and J.-M. Tarascon, *J. Electrochem. Soc.*, 149 (2002) A1212.
4. A. Débart, L. Dupont, P. Poizot, J-B. Leriche and J. M. Tarascon, *J. Electrochem. Soc.*, 148 (2001) A1266.
5. S. Y. Liu, J. Xie, Q. Pan, C. Y. Wu, G. S. Cao, T. J. Zhu and X. B. Zhao, *Int. J. Electrochem. Sci.*, 7 (2012) 354.
6. X. H. Huang, J. P. Tu, X. H. Xia, X. L. Wang, J. Y. Xiang, L. Zhang and Y. Zhou, *J. Power Sources*, 188 (2009) 588.
7. X. H. Huang, J. P. Tu, X. H. Xia, X. L. Wang and J. Y. Xiang, *Electrochem. Commun.*, 10 (2008) 1288.
8. Q. Pan, L. Qin, J. Liu and H. Wang, *Electrochim. Acta*, 55 (2010) 5780.
9. C. Q. Zhang, J. P. Tu, Y. F. Yuan, X. H. Huang, X. T. Chen and F. Mao, *J. Electrochem. Soc.*, 154 (2007) A65.
10. J. Liu, Y. Li, R. Ding, J. Jiang, Y. Hu, X. Ji, Q. Chi, Z. Zhu and X. Huang, *J. Phys. Chem. C*, (2009) 5336.
11. J. Liu, Y. Li, X. Huang, G. Li and Z. Li, *Adv. Funct. Mater.*, 18 (2008) 1448.

12. X. Tang, Q. Pan and J. Liu, *J. Electrochem. Soc.*, 157 (2010) A55.
13. J. H. Lee, M. H. Hon, Y. W. Chung and I. C. Leu, *Appl. Phys. A.*, 102 (2011) 545.
14. J. Wang, N. Du, H. Zhang, J. Yu and D. Yang, *Mater. Res. Bull.*, 46 (2011) 2378.
15. Y. N. Zhou, W. J. Li and Z. W. Fu, *Electrochim. Acta*, 59 (2012) 435.
16. H. Wang, Q. Pan, Y. Cheng, J. Zhao and G. Yin, *Electrochim. Acta*, 54 (2009) 2851.
17. G. Jo, H. Choi, H. Ahn, M and J. Park, *Chem. Commun.*, 48 (2012) 3987.
18. J. Wang, N. Du, H. Zhang, J. Yu and D. Yang, *J. Power Sources*, 208 (2012) 434.
19. G. Gachot, S. Grugeon, M. Armand, S. Pilard, P. Guenot, J.-M. Tarascon and S. Laruelle, *J. Power Sources*, 178 (2008) 409.